IOPscience iopscience.iop.org

Home Search Collections Journals About Contact us My IOPscience

Phase behaviour and quasi-one dimensionality of betaine arsenate/phosphate mixed crystals

This article has been downloaded from IOPscience. Please scroll down to see the full text article.

1996 J. Phys.: Condens. Matter 8 4617

(http://iopscience.iop.org/0953-8984/8/25/017)

View the table of contents for this issue, or go to the journal homepage for more

Download details:
IP Address: 171.66.16.206
The article was downloaded on 13/05/2010 at 18:14

Please note that terms and conditions apply.

J. Phys.: Condens. Matter **8** (1996) 4617–4629. Printed in the UK

Phase behaviour and quasi-one dimensionality of betaine arsenate/phosphate mixed crystals

M Manger†, S Lanceros-Méndez†, G Schaack† and A Klöpperpieper‡

† Physikalisches Institut der Universität Würzburg, Am Hubland, D-97074 Würzburg, Germany
‡ Fachbereich Physik der Universität des Saarlandes, D-66123 Saarbrücken, Germany

Received 9 November 1995, in final form 28 March 1996

Abstract. The temperature dependence (24 K $< T <$ 300 K) of the complex permittivity $\epsilon = \epsilon' - i\epsilon''$ in a ferroelectric $BA_{0.73}BP_{0.27}$ mixed crystal has been studied. In order to tune the intermolecular dipolar interactions and to study the stability and kinetics of the different phases of the crystal under investigation, we performed measurements under application of hydrostatic pressures ($p <$ 350 MPa), biasing fields ($E <$ 8 kV cm^{-1}), and different measurement frequencies (0.1 kHz $\leqslant \nu \leqslant$ 100 kHz). These experiments allowed us to depict the corresponding pressure–temperature and electric field–temperature anomaly diagrams of the crystal investigated. Furthermore, in order to analyse the changes in the dipolar system accompanying the dielectric anomalies, we performed dielectric hysteresis measurements. These measurements finally enabled us to identify the character of the phase transitions and the corresponding changes in the dipole system accompanying the dielectric anomalies. A high-temperature transition into an antiferroelectrically ordered phase followed by a re-entrant glassy phase has been found. The high-temperature antiferroelectric transition is discussed in the framework of the quasi-one-dimensional Ising model and compared to the corresponding transitions of the pure compounds, ferroelectric betaine arsenate (BA) and antiferroelectric betaine phosphate (BP), respectively. The low-temperature transition into the re-entrant glassy phase is treated according to the frequency-dependent shift of its indicating anomaly by means of an Arrhenius versus Vogel–Fulcher analysis.

1. Introduction

Ferroelectric (F) betaine arsenate (BA, $(CH_3)_3NCH_2COO \cdot H_3AsO_4$) and antiferroelectric (AF) betaine phosphate (BP, $(CH_3)_3NCH_2COO \cdot H_3PO_4$) are salts of the amino acid betaine and the arsenic and phosphoric acids, respectively. As the two substances exhibit crystal structures that are almost the same, the mixed crystals BA_xBP_{1-x} can be grown from aqueous solution over the whole concentration range. The particular features of the system investigated, BA_xBP_{1-x}, are, on the one hand, the expected frustration of the dipole–dipole interactions due to the compositional disorder, leading possibly to a glasslike freezing of the dipoles in the intermediate-concentration range, while, on the other hand, there is the quasi-one-dimensional structure of the pure compounds, with the inorganic tetrahedral groups (arsenate, phosphate) linked by hydrogen bonds along the polar axis forming zigzag chains, which should also have a distinct influence on the phase behaviour of the mixed crystals [1, 2].

In order to get information about the identity and the stability of the polar phases of these crystals, we have performed dielectric measurements by applying both hydrostatic pressure [3, 4, 5, 6] and an electric bias field [7] along the polar axis to some mixed

0953-8984/96/254617+13$19.50 © 1996 IOP Publishing Ltd

crystals spread over the whole concentration range. Furthermore, we carried out dielectric hysteresis measurements under various hydrostatic pressures with some samples, thereby intending to characterize the changes in the dipolar system responsible for the anomalies in the real (ϵ') and the imaginary part (ϵ'') of the dielectric constant [8]. In addition, Raman and infrared spectroscopy was also applied in order to get information about the structural changes coinciding with the dipolar anomalies [9]. The crystals under investigation show a phase behaviour, which manifests itself in unusual and complex pressure–temperature–concentration phase diagrams [4, 5, 6]. Here we report on the experimental results obtained for a sample with a BA concentration $x = 0.73$. This crystal falls in the concentration range $0.5 < x < 0.8$ [6], where in spite of the BA dominance a transition occurs into an AF phase, and where the anomaly in $\epsilon'(T)$ indicative of the transition into the ordered phase splits under pressure developing a second shoulder-shaped anomaly. Characteristic for this region are also rather complicated and strangely shaped hysteresis loops with several polarization components superposing on the principal AF contribution, which we will present below. Furthermore, we have found low-temperature anomalies in $\epsilon''(T)$ attesting to the existence of freezing processes in the dipolar system. This freezing is due to compositional disorder and the resulting frustration of the dipole–dipole interactions interpreted by means of a transition into a re-entrant glassy phase.

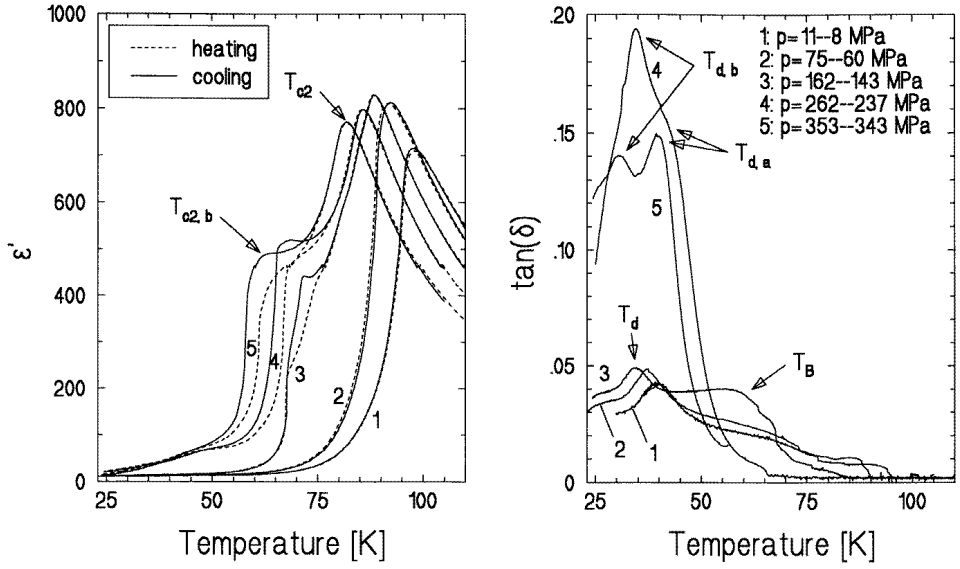

Figure 1. $\epsilon'(T)$ (left) and the corresponding $\tan\delta(T)$ curves (right) of $BA_{0.73}BP_{0.27}$ taken for several pressures and a measuring frequency $\nu = 100$ kHz on cooling and heating.

2. Experimental procedure

The crystals were grown by controlled evaporation from aqueous solution, and their concentrations subsequently analysed by means of UV spectroscopy and density methods to an accuracy of about 3%. Samples in the shape of thin slices ($d < 0.5$ mm) were oriented perpendicularly to the polar axis, and vacuum-deposited aluminium or gold films served as electrodes. Furthermore, from the good condition of all of the samples after

having experienced the straining pressure treatment, we conclude that there was a good concentration homogeneity in the samples.

The temperature (23−300 K), hydrostatic pressure ($p < 350$ MPa), and bias field ($E < 8$ kV cm^{-1}) dependence of $\epsilon'(T)$, and the dissipation factor $D(T) = \tan\delta(T) = \epsilon''(T)/\epsilon'(T)$ were measured at several frequencies 0.1 kHz $< \nu <$ 100 kHz with a standard LCZ meter (Keithley model 3322). Helium, which behaves hydrostatically even in the frozen state, was used as the pressure-transmitting medium. The bias field experiments were performed using a home-built circuit in order to resolve the imaginary part of the dielectric constant [10]. The measurements of the hysteresis loops and the current curves (derivatives of the hysteresis loops) were carried out by means of a hysteresis bridge based on operational amplifiers and a dc high-voltage amplifier [10]. This instrument detects the charge and discharge currents and subsequently integrates them by an analogue method to yield the dielectric polarization. With this method we could optionally record either the dielectric polarization or the charge current of the sample. The charge current thereby has, as compared to the polarization, the advantage of directly indicating the number of dipole reorientation processes at a certain electric field. It is therefore sometimes a more sensitive quantity for getting insight into the changes occurring in the dipolar system. The maximum voltage applied to the sample was experimentally limited to 1000 V and the frequencies used were 0.1, 1, 10, and 100 Hz.

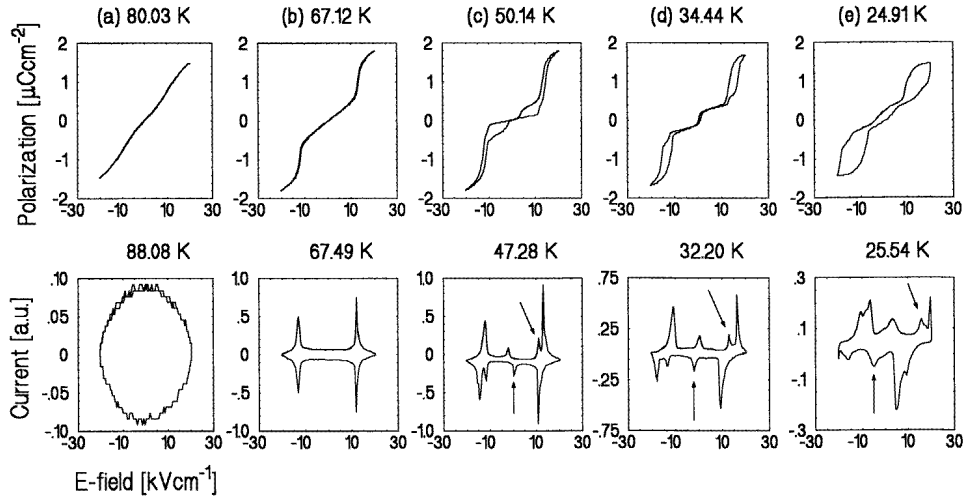

Figure 2. Typical hysteresis loops (above) and current curves (below) for $BA_{0.73}$ at $p \approx$ 350 MPa in the different temperature regimes (maximum field $E_{max} = 20.3$ kV cm^{-1}, measuring frequency $\nu = 10$ Hz, sinusoidal field variation). For orientation purposes the various anomaly temperatures are given: $T_{c2} \simeq 82$ K, $T_{c2,b} \simeq 60$ K, $T_{i,a} \simeq 41$ K, $T_{d,b} \simeq 30$ K.

3. The influence of hydrostatic pressure

The temperature dependence of ϵ' and $\tan\delta$ is shown in figure 1 for several hydrostatic pressures at a measuring frequency $\nu = 100$ kHz. In figure 2 we show some representative hysteresis and current loops obtained at $p \simeq 350$ MPa.

From these figures one can draw the following conclusions: at all pressures there appears

a dominant anomaly at a temperature T_{c2} in $\epsilon'(T)$, indicating the transition into an AF phase. This type of ordering becomes evident from the characteristically shaped hysteresis loop in figure 2(b), which in the corresponding temperature regime is representative for the whole pressure region under study. Thus, surprisingly, the type of ordering is determined by the partner with the lower concentration (BP). No thermal hysteresis can be observed for this transition and it is of second order, as the influence of the bias field will show in section 5. With increasing pressure the ordered phase is clearly destabilized, as are both the F phase of pure BA and the AF phase of pure BP [3, 6], leading to a shift of the transition temperature T_{c2} (T_{c1} being the transition temperature of the nonpolar purely structural high-temperature transition [1, 2]) to lower values. The broad and rather diffuse shape of the anomaly is supposed to be caused by locally differing transition temperatures due to concentration fluctuations.

Above a critical pressure 75 MPa $< p_{c1} <$ 150 MPa, a shoulder-like structure develops on the low-temperature side of the T_{c2} anomaly. This structure shows a large thermal hysteresis (figure 1) concerning its position $T_{c2,b}$ (the point of strongest curvature) and its shape. Looking at the dielectric hysteresis loops in the corresponding $p-T$ region one can recognize a drastic change in their shape, indicating a reorientation process in the dipolar system (figure 2(c)). This change is attributed to a second phase transition of mainly first-order character, due to the strong thermal hysteresis of the $T_{c2,b}$-shoulder. The changes concerning this shoulder can be analysed more accurately by evaluating the corresponding current curves. Here, in addition to the sharp peaks originating from the field-induced AF-to-F transition (dominant peaks) both in the activation (region of increasing field) and in the relaxation (with decreasing field) regions of the current loops, new peaks (arrows in figures 2(c) 2(d) and 2(e))) appear. Whereas the relaxation and the activation peak of the forced AF-to-F transition occur almost at the same position on the electric field axis, leading in the temperature region $T_{c2,b} < T < T_{c2}$ to almost closed hysteresis loops (figure 2(b)), the positions of the new activation and relaxation peaks differ strongly, resulting in strangely opened loops (figures 2(c) and 2(d)). The peak sharpness and the clear correlation between the marked activation and relaxation peak lead us to the conclusion that either a new collectively ordering dipole system appears or, more probably, that the original dipole system splits into two separately ordering parts. There is obviously a tendency for the original system to maintain at least partially its AF order, whereas the new system tends to develop a remanent polarization at lower temperatures (figure 2(d)), thus carrying pseudo-F character. The onset of the remanent polarization is, however, not accompanied by an anomaly in $\epsilon'(T)$; thus it concerns a feature based essentially on the dipole relaxation. The contributions of the two dipolar systems to the spontaneous polarization remain roughly independent of temperature (figure 2) and pressure (not shown).

At lower temperatures the response of the system is mainly dominated by the behaviour of $\tan\delta(T)$ or $\epsilon''(T)$, respectively. In this region the curves can also be divided into a low- and a high-pressure behaviour: whereas at low pressures there is only one anomaly sitting on a relatively high background, two strong anomalies emerge at high pressure (figure 1). Obviously, since the shoulder-shaped anomaly ($T_{c2,b}$) already exists at $p \simeq 150$ MPa and the low-temperature behaviour is still identical with that at low pressures, there should be another critical pressure p_{c2} between 150 and 250 MPa where mainly the kinetics of the system, revealing itself in the dielectric losses, changes. The processes occurring in the dipolar system again become accessible in the corresponding hysteresis and current curves, where one can recognize that the anomaly emerging in $\tan\delta(T)$ at the higher temperature $T_{d,a}$ marks the onset of a remanent polarization (the same change manifests itself in a similar

anomaly in the corresponding $\epsilon''(T)$ curves at the shifted temperature $T_{i,a}$†). Simultaneously the relaxation peak in the current curves (figure 2) attributed to the second dipole system passes the zero-field axis, clearly identifying the second dipole system as responsible for this change. At intermediate pressures, i.e. in the transition region $p_{c1} < p = 150$ MPa $< p_{c2}$, the features, which are not presented here, are much more complicated and difficult to overlook. However, the enhancement in $\tan\delta(T)$ at $T \simeq 60$ K (denoted as T_B in figure 1) seems to be indicative for a change in the dipole system similar to the change at high pressures.

Qualitatively similar results have been obtained for a crystal with a BA concentration $x = 0.62$, which is located in the same area of the temperature–concentration phase diagram [8]. The evolution of these complex loops from simple AF or F loops in pure BP and BA, respectively, can be rather well followed in concentration, allowing a better understanding of the dielectric ordering in the BA_xBP_{1-x} system. A more complete analysis of the hysteresis and current curves over the whole concentration range will be presented soon [8].

As will be elaborated in section 6 in the investigation of the frequency dispersion, the anomalies T_d (equivalent to T_i) at low pressure and $T_{d,b}$ (i.e. $T_{i,b}$) at high pressure seem to be of the same origin and therefore indicative for a related change in the dipole kinetics. Furthermore, both anomalies shift in an almost parallel fashion with T_{c2} under pressure, hinting at a relation to the original AF order. From the polarization and current curves at $p = 350$ MPa, one can conclude that the corresponding change concerns mainly the original antiferroelectrically ordering dipole system: the peaks attributed to the second dipole system can still be clearly identified, whereas the formerly dominating peaks indicating the field-induced AF-to-F transition become more and more diffuse, leading to a drastic increase of the critical field, at which the induced AF-to-F transition takes place. Finally, saturation cannot be reached any longer and an opening of the hysteresis loops can be observed just below $T_{d,b}$. As will be outlined later in the treatment of the frequency dispersion, we attribute the lowest-lying anomaly to a transition into a glassy state where the former long-range order of the dipoles breaks down, at least partially.

4. Quasi-one dimensionality

According to the significant curvature of the $\epsilon'(T)$ curves in the Curie representation at the various pressures (figure 3), the transition into the antiferroelectrically ordered phase cannot be described with a classical Curie–Weiss law. However, the bowed curves can be quite well fitted with the quasi 1-D Ising model [11, 12, 13]. This model takes into account a chainlike structure where the interactions $J_\parallel$ between nearest-neighbour dipoles within the same chain are supposed to be unique and strongly ferroelectric, and are therefore treated exactly within the framework of the 1-D Ising model. The dipoles of different chains are only weakly coupled in a long-range mean-field way. An AF phase can be reproduced according to this model by considering two types of chain establishing opposite orientations of the polarization, with the chains of the same type coupling ferroelectrically and the chains of different type coupling antiferroelectrically. $J_\perp^{\alpha\alpha} > 0$ and $J_\perp^{\alpha\beta} < 0$ denote the corresponding interaction constants measured in temperature units for the chains of the same and different types, respectively. This model is applied successfully to the pure substances BA [14] and BP [15] and therefore it is the most self-suggesting model yielding deviations from the classical Curie–Weiss behaviour also for the mixed crystals.

† The subscripts 'd' and 'i' refer to whether an anomaly is considered in $\tan\delta(T)$ or ϵ'', respectively, whereas a second subscript 'a' or 'b' serves to distinguish different anomalies.

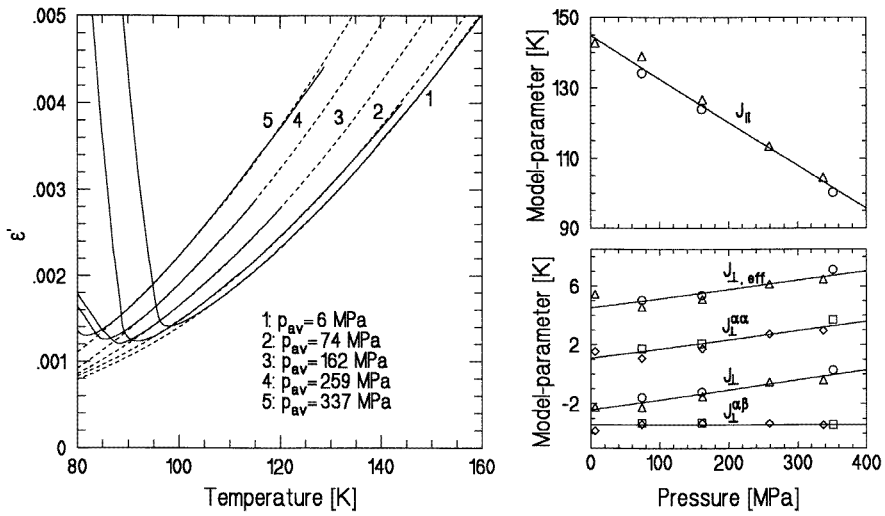

Figure 3. Left: a Curie representation of $\epsilon'(T)$ at different pressures and $\nu = 100$ kHz on heating (full lines) and the corresponding fits (broken lines). Right: the pressure dependence of the fitted parameters. Circles and squares: on cooling; diamonds and triangles: on heating.

For testing its applicability, the experimental $\epsilon'(T)$ curves were fitted in the temperature regions $T > T_{c2}(p) + (\simeq 5\ \mathrm{K})$ according to the equation [12, 13]

$$\epsilon'(T) = \epsilon_\infty + \frac{C}{T}\left[\exp\left(\frac{-2J_\parallel}{T}\right) - \frac{J_\perp}{T}\right]^{-1} \tag{1}$$

which is valid either in the F or AF case. ϵ_∞ thereby takes into account a temperature-independent background permittivity, C denotes the Curie constant, being a direct measure for the effective dipolar moment, and $J_\parallel$ and $J_\perp = J_\perp^{\alpha\alpha} + J_\perp^{\alpha\beta}$ represent the intrachain and interchain interactions, respectively. As the experimental curves tend with $T \to 0$ to very small values as compared to the height of the anomaly marking the AF transition, the background ϵ_∞ was neglected in the fitting procedure. Furthermore, the Curie constant C was held, according to the results from preliminary fits, at a unique intermediate value of $C = 5800$ K. Finally, the interaction constants $J_\parallel$ and $J_\perp$ were the only parameters to be varied in the fitting procedure. Together with having the implicit expression for the phase transition temperature $T_c \equiv T_{c2}$ [12, 13]

$$\exp\left(\frac{-2J_\parallel}{T_c}\right) = \frac{J_\perp^{\alpha\alpha} + |J_\perp^{\alpha\beta}|}{T_c} = \frac{J_{\perp,eff}}{T_c} \tag{2}$$

we were able to perform a parametrization of the crystal investigated according to the above-mentioned model. Note that the effective interaction strength $J_{\perp,eff}$, determining the phase transition temperature, is only in the F case identical with the corresponding parameter $J_\perp$ of the fitting equation. Thus in the F case it is probably not necessary to distinguish between different kinds of chain. In the AF case, however, due to the negative sign of $J_\perp^{\alpha\beta}$, one has to take the results from the fit and the evaluation of the transition temperature simultaneously into account, for determining the interactions $J_\perp^{\alpha\alpha}$ and $J_\perp^{\alpha\beta}$.

The results of the parametrization are also shown in figure 3 as a function of the hydrostatic pressure. We obtained an almost linear dependence of the interaction constants

on the applied pressure, which can be described by the following relations:

$$\begin{aligned} J_{\parallel}(p) &= 145\ \mathrm{K} - 123\ \frac{\mathrm{K}}{\mathrm{GPa}}\ p \\ J_{\perp}^{\alpha\alpha}(p) &= 1.1\ \mathrm{K} + 6.3\ \frac{\mathrm{K}}{\mathrm{GPa}}\ p \\ J_{\perp}^{\alpha\beta}(p) &= -3.4\ \mathrm{K}. \end{aligned} \tag{3}$$

The behaviour of the parameters indicates according to equation (1) that the observed shift of T_{c2} to lower values with increasing pressure is fully due to the strong drop of the intrachain interaction $J_{\parallel}$ as the effective interchain interaction strength [12, 13] $J_{\perp,eff} = J_{\perp}^{\alpha\alpha} + |J_{\perp}^{\alpha\beta}|$ in contrast increases with pressure, tending to stabilize the AF order. Hence the strengthening of the interchain interactions with rising pressure is fully overcompensated in its effect by the strong decrease of the intrachain interactions.

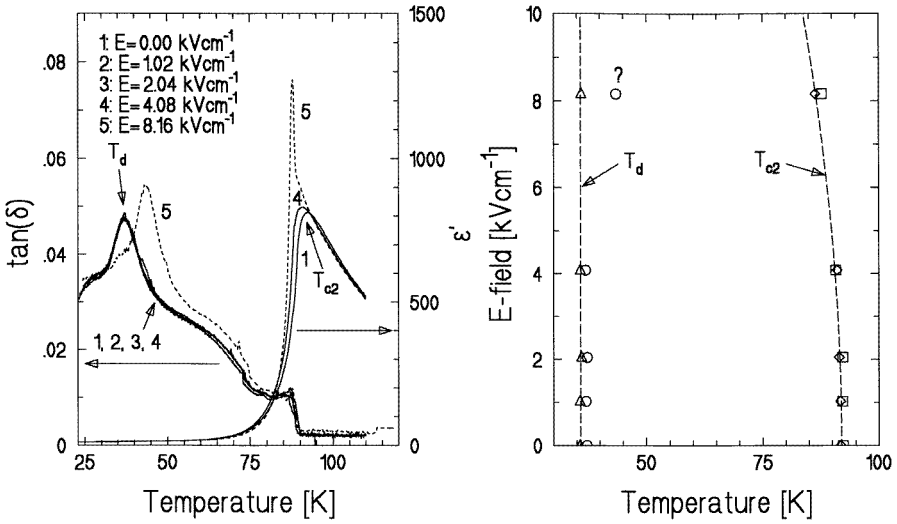

Figure 4. Left: $\epsilon'(T)$ and $\tan\delta(T)$ curves for several bias fields, $p \approx 75$ MPa, $\nu = 100$ kHz, and cooling. Right: the corresponding $E-T$ anomaly diagram. Circles and squares: cooling; diamonds and triangles: heating. T_{c2} shifts approximately with the square of the field: T_{c2} (K) $= 92.0 - 8.2 \times 10^{-2}(E\ (\mathrm{kV\ cm^{-1}}))^2$. Curve number 5 on cooling shows an anomalous thermal hysteresis in $\tan\delta$, i.e. $\epsilon''(T)$. This cannot be explained but is supposed to be an experimental error.

The quasi-one dimensionality and the weakening of the intrachain interaction with pressure indicate the importance of the H bonds in the phase transition mechanism. The pressure behaviour must be mainly caused by the chain-forming H bonds as they represent the weakest and therefore the most easily influenceable bonds in the crystal. The shortening of the H bonds by compressing the crystal leads in a tentative picture to a lowering of the potential well between the two equilibrium sites of the protons.

This lowering results on the one hand in the frame of the tunnelling model in an increase of the tunnelling rate through the barrier and therefore a destabilization of the order. Tunnelling might play a certain role in this system as the H-bond lengths of the pure compounds lie around the 2.5 Å, a region where according to theoretical considerations tunnelling should occur.

On the other hand, without referring to the tunnelling picture, the destabilization can be explained by an increase of the thermal hopping probability for the protons with decreasing barrier height. For a discussion of the results obtained for the pure compounds from this point of view and a comparison with other systems, see [3]. Although the H bonds, as the polarization measurements on the pure compounds have shown, have only an almost negligible contribution to the molecular dipole moment per unit cell, they seem to be the mediators of the intrachain interactions in the BA_xBP_{1-x} system. Comparing to the parameters of the pure systems (BA: $C = 8500$ K, $J_{\parallel} = 183$ K, $J_{\perp} = 5.7$ K [14]; BP: $J_{\parallel} = 84$ K, $J_{\perp}^{\alpha\alpha} = 2.3$ K, $J_{\perp}^{\alpha\beta} = -9.8$ K [15] at atmospheric pressure), those of our crystal fall into reasonable intermediate ranges, thus confirming the applicability of the quasi 1-D Ising model to our sample.

The interchain parameters, according to the observed AF order, are dominated by the contributions of the BP groups, but fluctuations of these interactions in the mixed crystals in the order of magnitude of their average values should be expected. Therefore frustration effects should be strong and have a drastic influence especially on the low-temperature behaviour, possibly leading to a glasslike freezing of the dipoles. This topic will be illuminated in more detail in the last section.

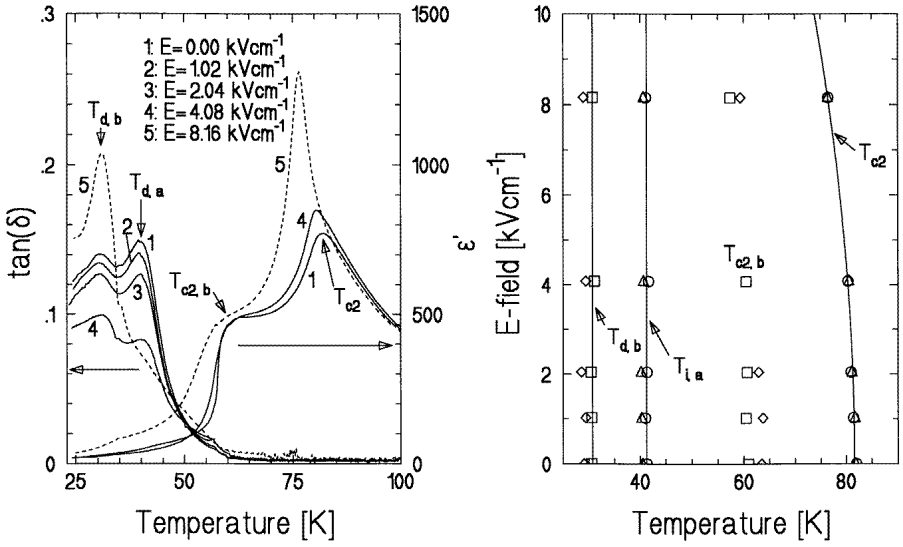

Figure 5. Left: $\epsilon'(T)$ and $\tan\delta(T)$ curves for several bias fields, $p \approx 350$ MPa, $\nu = 100$ kHz, and cooling. Right: the corresponding $E-T$ anomaly diagram. Circles and squares: cooling; diamonds and triangles: heating. T_{c2} shifts approximately with the square of the field: T_{c2} (K) $= 81.6 - 7.8 \times 10^{-2}(E$ (kV cm^{-1}))^2.

5. The influence of an external bias field

The dielectric curves measured at different bias fields are shown for two pressures $p \simeq 70$ MPa and $p \simeq 350$ MPa together with the evaluated anomaly diagrams in figures 4 and 5, respectively. Figure 6 serves as a comparison of the zero-field curves with those at the highest applied field. The main effect of the external field is a shift of the transition

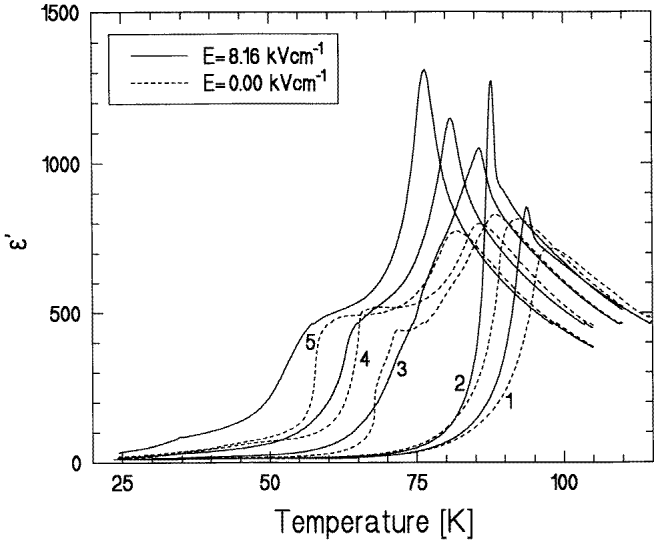

Figure 6. $\epsilon'(T)$ at different pressures for $E = 0$ kV cm^{-1} (broken lines) and $E = 8.16$ kV cm^{-1} (full lines), $\nu = 100$ kHz, and cooling. 1: $p \approx 10$ MPa, 2: $p \approx 60$ MPa, 3: $p \approx 150$ MPa, 4: $p \approx 250$ MPa, and 5: $p \approx 350$ MPa.

temperature T_{c2} to lower values, indicating the expected destabilization of the AF order. This shift can be described quite well by a quadratic dependence on the field, with the shift parameter $\mathrm{d}T_{c2}/\mathrm{d}(E^2)$ being approximately 8×10^{-2} K cm^2 kV^{-2} for all pressures. With increasing fields the anomaly also becomes sharper, leading at the highest applied field, particularly at the two lowest pressures, to a clearly enhanced cusp. This cusp combined with the quadratic field dependence of the peak position is typical for an AF phase transition of second order according to the classical theory of Kittel [16].

The shoulder-like anomaly appearing at high pressures smears out with increasing field strength and shifts slightly to lower temperatures; thus it is also destabilized.

At low pressures $p < p_{c1}$, the electric field has almost no influence either on the shape or on the position of the single anomaly T_d in $\tan\delta(T)$. On the other hand, the influence of the field on $\tan\delta(T)$ and $\epsilon''(T)$, respectively, is remarkable at high pressures (figure 5): the height of the two peaks changes drastically with increasing field in favour of the low-lying anomaly, whereas the peak positions $T_{d,a}$ and $T_{d,b}$ remain unaffected. With the help of the external field we are thus able for $p > p_{c2}$ to tune the mechanisms responsible for the corresponding anomaly without shifting its position.

6. Frequency dispersion

Looking for the possibility of a glasslike freezing of the dipoles due to randomly frustrated interactions we shall now discuss the frequency dependence of the dielectric constant. The measurements showed a remarkable frequency dispersion in $\epsilon'(T)$ coinciding with the low-temperature anomalies in $\tan\delta(T)$ and $\epsilon''(T)$, respectively. In order to characterize the changes in the dipole kinetics at low temperatures, we have evaluated the frequency dependence of the peak positions T_f ($\equiv T_i, T_{i,a}, T_{i,b}$) in $\epsilon''(T)$ and fitted them with the

Table 1. Parameters obtained from the Arrhenius and Vogel–Fulcher fits for the different anomalies T_i, $T_{i,a}$, and $T_{i,b}$.

Anomaly	Curve number	E (kV cm^{-1})	p (MPa)	ν_0 (Hz)	E_a/k_B (K)	T_{VF} (K)
T_i	1	0	9	4.3×10^9	265	15.2
T_i	2	0	64	2.9×10^9	208	17.4
T_i	3	0	145	1.4×10^9	156	18.4
$T_{i,b}$	4	8.16	239	5.2×10^9	171	18.5
$T_{i,b}$	5	8.16	341	8.2×10^{10}	295	10.3
$T_{i,a}$	6	0	245	4.4×10^{18}	1380	0
$T_{i,a}$	7	0	344	5.2×10^{16}	1120	0

empirical Vogel–Fulcher formula

$$\nu = \nu_0 \exp\left(-\frac{E_a}{k_B(T_f - T_{VF})}\right). \tag{4}$$

This formula is an extension of the well known Arrhenius law, which describes the probability for a particle to make a thermally activated jump over a hindering barrier of height E_a, with the proportionality constant ν_0 denoting the hopping frequency for the limiting case $T \to \infty$. The Vogel–Fulcher temperature T_{VF} was introduced to take phenomenologically into account the influence of nonthermal effects on the collective dynamics of the system. This Vogel–Fulcher behaviour is often applied to describe the frequency shift of the freezing peak in dipole glasses, and therefore T_{VF} is often taken to define the proper equilibrium (zero-frequency) freezing temperature of such systems.

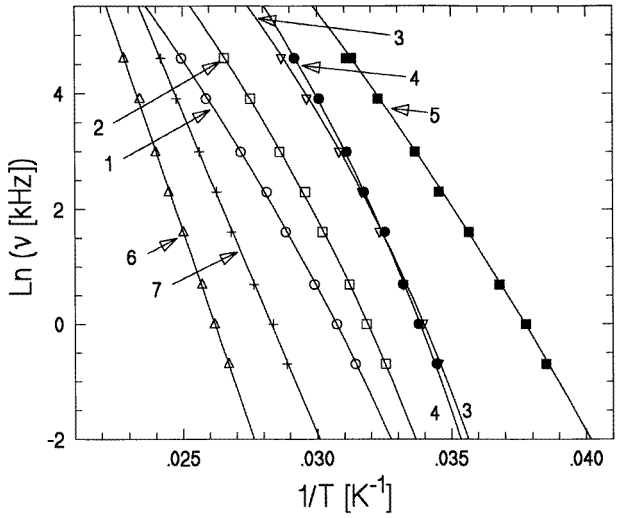

Figure 7. An Arrhenius plot of the frequency-dependent positions of the $\epsilon''(T)$ anomalies. The corresponding values of the pressure and the field are indicated in table 1.

The results of this evaluation are tabulated in table 1 and graphically represented in the form of an Arrhenius plot in figure 7. In spite of the small number of experimental

points, one can attribute a Vogel–Fulcher behaviour to the anomalies T_i ($p < p_{c2}$) and $T_{i,b}$ ($p > p_{c2}$) and an Arrhenius behaviour to the anomaly $T_{i,a}$. The anomaly $T_{i,b}$ was evaluated for this purpose at the highest applied bias field, where its height is drastically raised but its position not shifted. The values of the parameters E_a and T_{VF} fit together well in the interface region $p \rightarrow p_{c2}^{\pm}$, confirming that both anomalies represent an equivalent change in the dipolar system. Considering them as equivalent, the pressure-induced change in the system expresses itself in a minimum of the activation energy E_a and simultaneously in a maximum of the Vogel–Fulcher temperature. The frequencies ν_0 lie in the microwave regime.

The second anomaly $T_{i,a}$, emerging at high pressures and being attributed primarily to a change in the second dipole system, obeys an Arrhenius law with quite high frequencies ν_0. This fact cannot be explained at the moment, as the origin of the second dipole system is not clear.

An anomaly behaving in a Vogel–Fulcher-type fashion in $\epsilon''(T)$ which is accompanied by an onset of frequency dispersion in $\epsilon'(T)$ is, as mentioned above, typically observed in dipole glasses. The values obtained also agree as regards order of magnitude with those obtained for other dipole glasses, e.g. $K_{0.77}(NH_4)_{0.23}H_2AsO_4$: $T_{VF} = 8.3$ K, $E_a = 183.5$ K and $\nu_0 = 1.65 \times 10^{11}$ Hz [17]. We interpret our observations concerning the anomalies T_i and $T_{i,b}$ with a re-entrant glass transition taking place in the original AF ordered dipole system at T_{VF}. From the results in section 4 strong fluctuations of the interchain interactions in the order of their average value are to be expected. This seems to be an acceptable explanation for the observed features. It is striking in this context that the supposed glassy phase is extremely stable against the applied bias field, manifesting itself in a nearly field-independent position of the glass-indicating anomalies.

7. Summary and conclusions

Measurements of the complex dielectric permittivity at several frequencies and recordings of the dielectric hysteresis and current curves have been carried out for a $BA_{0.73}BP_{0.27}$ mixed crystal by changing external parameters like temperature, pressure, and external bias field. Different phases, revealing themselves through anomalies in the dielectric response, have been analysed by means of their sensitivity to the experimentally varied external parameters and their characteristic hysteresis and current loops. The results obtained can be summarized in the form of the temperature–pressure phase diagram presented in figure 8.

Like at other concentrations in the BA_xBP_{1-x} system, the pressure–temperature phase diagrams can be divided into two main regions: a transition into a polar ordered phase at higher temperatures, and a further lower-temperature region marked by anomalies in $\epsilon''(T)$ and $\tan\delta(T)$ and a strong frequency dispersion, indicating a relaxational process in a probably glassy phase. The higher-temperature AF transition was discussed in the framework of the quasi-1D Ising model, and the observed destabilization with increasing pressure was explained by the easy influenceability of the chain-forming hydrogen bonds.

Under pressure, additional structures observable in $\epsilon''(T)$ or $\tan\delta(T)$, respectively, arise. These structures were interpreted by the appearance of a second dipole system, partially carrying F character and being responsible for the drastic deformation of the hysteresis loops, whose origin is still not clear. Furthermore we found out that the development of the second dipole system occurs in two steps, each being marked by a critical pressure.

The behaviour at lower temperatures is dominated by structures in $\tan\delta(T)$ (i.e. $\epsilon''(T)$) and a frequency dispersion in $\epsilon'(T)$. The frequency shift of the anomalies was investigated by means of a Vogel–Fulcher versus Arrhenius analysis. An anomaly behaving in a Vogel–

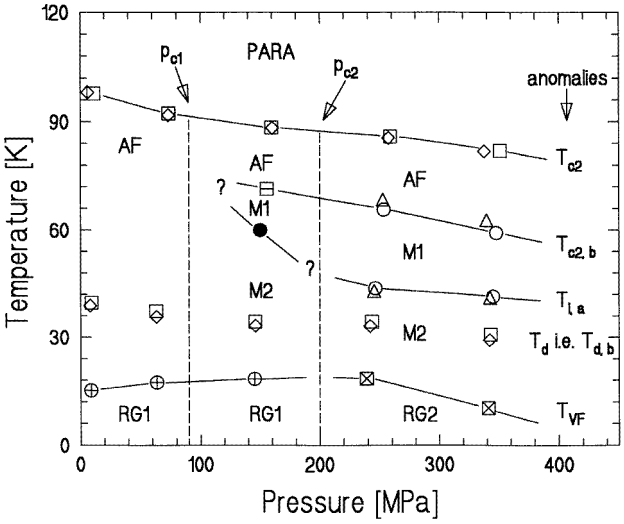

Figure 8. A $T-p$ phase diagram for $BA_{0.73}BP_{0.27}$. The points are evaluated from the positions of the maxima and shoulders in figure 1 or taken from table 1, respectively. AF: antiferroelectric phases; M1 and M2: phases in which the two dipolar systems coexist; RG1 and RG2: re-entrant glassy phases. p_{c1} and p_{c2} (broken lines) represent approximately the critical pressures above which pressure-induced transitions occur. Circles and squares: cooling; diamonds and triangles: heating. The lines connecting the points representing the same transition at different pressures are guides for the eyes.

Fulcher-type fashion, which is present at all pressures, was interpreted in terms of a transition into a re-entrant glassy phase, with the former AF long-range order breaking down at least partially.

As qualitatively analogous results for a $BA_{0.62}BP_{0.38}$ crystal indicate [8], our conclusions seem to be valid over a broader intermediate-concentration range. Similar analysis for several samples over the whole concentration range will allow us to present a more complete picture of the BA_xBP_{1-x} system in the near future.

Acknowledgment

The support from the Basque Government under grant BFI94.092 is gratefully acknowledged by SLM.

References

[1] Schildkamp W and Spilker J 1984 *Z. Kristallogr.* **168** 159
[2] Schildkamp W, Schäfer G and Spilker J 1984 *Z. Kristallogr.* **168** 187
[3] Launer S, le Maire M, Schaack G and Haussühl S 1992 *Ferroelectrics* **135** 257
[4] Lanceros-Méndez S, le Maire M, Schaack G, Schmitt-Lewen M and Wilhelm C 1994 *Ferroelectrics* **157** 269
[5] Lanceros-Méndez S, Schaack G and Klöpperpieper A 1996 *Proc. 3rd Int. Symp. on Domain Structure of Ferroelectrics and Related Materials, ISFD-3 (1994); Ferroelectrics* at press
[6] Lanceros-Méndez S, Schaack G, Köhler M, Klöpperpieper A 1996 *Proc. 2nd Workshop on Low-Energy Dynamics in Solids, LEES-2 (1995); Ferroelectrics* at press

[7] Lanceros-Méndez S, Manger M, Schaack G and Klöpperpieper A 1996 *Proc. 8th European Mtg on Ferroelectricity, EMF-8 (1995); Ferroelectrics* at press
[8] Köhler M, Lanceros-Méndez S, Schaack G and Klöpperpieper A, to be published
[9] Lanceros-Méndez S, Ebert H and Schaack G 1996 *Proc. 14th Int. Conf. on Raman Spectroscopy (1994)* ed N-T Yu and X-Y Li (New York: Wiley) at press
[10] Manger M 1994 *Diploma Thesis* University of Würzburg
[11] de Carvalho A V and Salinas S R 1978 *J. Phys. Soc. Japan* **44** 238
[12] Blinc R, Žekš B, Levstik A, Filipic C, Slak J, Burgar M, Zupancic I, Shuvalov L A and Baranov A I 1979 *Phys. Rev. Lett.* **43** 231
[13] Blinc R and Sa Barreto F C 1980 *J. Chem. Phys.* **72** 6031
[14] Müser H E and Schell U 1984 *Ferroelectrics* **55** 279
[15] Fischer G, Brückner H J, Klöpperpieper A, Unruh H G and Levstik A 1990 *Z. Phys.* B **79** 301
[16] See, for example,
Lines M E and Glass A M 1977 *Principles and Applications of Ferroelectrics and Related Materials* (Oxford: Clarendon)
[17] Trybula Z, Los S, Tu C S and Schmidt V H 1995 *J. Phys.: Condens. Matter* **7** 947